Supplementary Information for "Structure-property relationships and the mechanisms of multistep transitions in spin crossover materials and frameworks"

Jace Cruddas* and B. J. Powell†
School of Mathematics and Physics, The University of Queensland, QLD 4072, Australia

S1. EXPANSION OF THE POTENTIAL

In the main text (Eq. 3) we consider a pairwise potential between neighbouring metal cites that depends on the spin spin-states of the metal ions, σ_i and σ_j. This potential is given by

$$V_{ij}(r,\sigma_i,\sigma_j) = g_{ij}(r) + h_{ij}(r)\left[r - \eta_{ij}\left\{\overline{R} - \delta(\sigma_i+\sigma_j)\right\}\right] + \frac{1}{2}k_{ij}(r)\left[r - \eta_{ij}\left\{\overline{R} - \delta(\sigma_i+\sigma_j)\right\}\right]^2, \tag{S1}$$

where $\eta_{ij} = \eta_n = 1, \sqrt{2}, 2, \sqrt{5}, 2\sqrt{2}, \ldots$ is the ratio of distances between the nth and 1st nearest-neighbour distance on the undistorted square lattice.

We interpolate $V_{ij}(r,\sigma_i,\sigma_j)$ by introducing a new function $V_{ij}(r)$ defined such that $V_{ij}(r_H) = V_{ij}(r_H,1,1)$, $V_{ij}(r_L) = V_{ij}(r_L,-1,-1)$, and $V_{ij}(\overline{R}) = V_{ij}(\overline{R},1,-1) = V_{ij}(\overline{R},-1,1)$, which yields

$$\begin{aligned} g_{ij}(r) =& V_{ij}(r-\overline{R}\eta_{ij}) - \left(r-\overline{R}\eta_{ij}\right)\left(\frac{\left(V_{ij}(r-\overline{R}\eta_{ij}+2\delta\eta_{ij}) - V_{ij}(r-\overline{R}\eta_{ij}-2\delta\eta_{ij})\right)}{4\delta\eta_{ij}}\right) \\ &+ \frac{1}{2}\left(r-\overline{R}\eta_{ij}\right)^2\left(\frac{\left(V_{ij}(r-\overline{R}\eta_{ij}+2\delta\eta_{ij}) - 2V_{ij}(r-\overline{R}\eta_{ij}) + V_{ij}(r-\overline{R}\eta_{ij}-2\delta\eta_{ij})\right)}{(2\delta\eta_{ij})^2}\right), \end{aligned} \tag{S2}$$

$$\begin{aligned} h_{ij}(r) =& \left(\frac{\left(V_{ij}(r-\overline{R}\eta_{ij}+2\delta\eta_{ij}) - V_{ij}(r-\overline{R}\eta_{ij}-2\delta\eta_{ij})\right)}{4\delta\eta_{ij}}\right) \\ &- \left(r-\overline{R}\eta_{ij}\right)\left(\frac{V_{ij}(r-\overline{R}\eta_{ij}+2\delta\eta_{ij}) - 2V_{ij}(r-\overline{R}\eta_{ij}) + V_{ij}(r-\overline{R}\eta_{ij}-2\delta\eta_{ij})}{(2\delta\eta_{ij})^2}\right), \end{aligned} \tag{S3}$$

and

$$k_{ij}(r) = \frac{V_{ij}(r-\overline{R}\eta_{ij}+2\delta\eta_{ij}) - 2V_{ij}(r-\overline{R}\eta_{ij}) + V_{ij}(r-\overline{R}\eta_{ij}-2\delta\eta_{ij})}{(2\delta\eta_{ij})^2}. \tag{S4}$$

Noting that

$$V\left(r-\overline{R}\eta_{ij}+2\delta\eta_{ij}\right) = \sum_{n=0}^{\infty} V^{(n)}\left(r-\overline{R}\eta_{ij}\right)\frac{(2\delta\eta_{ij})^n}{n!}, \tag{S5}$$

where

$$V^{(n)}(x) \equiv \left(\frac{\partial^n V(r)}{\partial r^n}\right)\Big|_{r=x}, \tag{S6}$$

* j.cruddas@uq.edu.au
† powell@physics.uq.edu.au

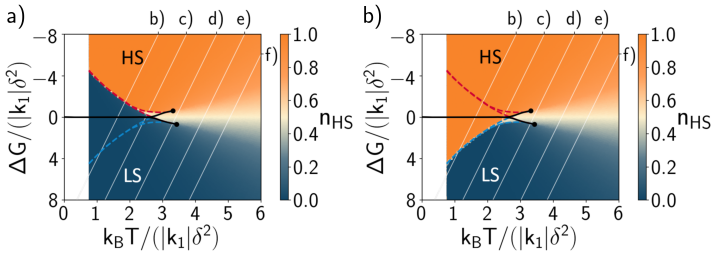

FIG. S1. The HS fraction, n_{HS}, calculated on (a) cooling and (b) heating for the nearest neighbour square lattice model with $k_1 > 0$. Lines and dots have the same meanings as in Fig. S2a, where we show the full phase diagram.

we find, with no further approximation, that

$$g_{ij}(r) = V_{ij}(r - \overline{R}\eta_{ij}) - (r - \overline{R}\eta_{ij}) \sum_{n=0}^{\infty} \frac{(2\delta\eta_{ij})^{2n}}{(2n+1)!} V_{ij}^{(2n+1)} (r - \overline{R}\eta_{ij}) + (r - \overline{R}\eta_{ij})^2 \sum_{n=1}^{\infty} \frac{(2\delta\eta_{ij})^{2(n-1)}}{(2n)!} V_{ij}^{(2n)} (r - \overline{R}\eta_{ij}) \quad \text{(S7)}$$

$$= V_{ij}(r - \overline{R}\eta_{ij}) - (r - \overline{R}\eta_{ij}) V_{ij}^{(1)} (r - \overline{R}\eta_{ij}) + \frac{(r - \overline{R}\eta_{ij})^2}{2} V_{ij}^{(2)} (r - \overline{R}\eta_{ij})$$
$$- (r - \overline{R}\eta_{ij}) \frac{2(\delta\eta_{ij})^2}{3} V_{ij}^{(3)} (r - \overline{R}\eta_{ij}) + (r - \overline{R}\eta_{ij})^2 \frac{(\delta\eta_{ij})^2}{6} V_{ij}^{(4)} (r - \overline{R}\eta_{ij}) + \ldots \quad \text{(S8)}$$

$$h_{ij}(r) = \sum_{n=0}^{\infty} \frac{(2\delta\eta_{ij})^{2n}}{(2n+1)!} V_{ij}^{(2n+1)} (r - \overline{R}\eta_{ij}) - 2(r - \overline{R}\eta_{ij}) \sum_{n=1}^{\infty} \frac{(2\delta\eta_{ij})^{2(n-1)}}{(2n)!} V_{ij}^{(2n)} (r - \overline{R}\eta_{ij}), \quad \text{(S9)}$$

$$= V_{ij}^{(1)} (r - \overline{R}\eta_{ij}) - (r - \overline{R}\eta_{ij}) V_{ij}^{(2)} (r - \overline{R}\eta_{ij}) + \frac{2(\delta\eta_{ij})^2}{3} V_{ij}^{(3)} (r - \overline{R}\eta_{ij}) - (r - \overline{R}\eta_{ij}) \frac{(\delta\eta_{ij})^2}{3} V_{ij}^{(4)} (r - \overline{R}\eta_{ij}) + \ldots \quad \text{(S10)}$$

$$k_{ij}(r) = 2 \sum_{n=1}^{\infty} \frac{(2\delta\eta_{ij})^{2(n-1)}}{(2n)!} V_{ij}^{(2n)} (r - \overline{R}\eta_{ij}) \quad \text{(S11)}$$

$$= V_{ij}^{(2)} (r - \overline{R}\eta_{ij}) + \frac{(\delta\eta_{ij})^2}{3} V_{ij}^{(4)} (r - \overline{R}\eta_{ij}) + \ldots \quad \text{(S12)}$$

To reach Eqs. 4 and 5 of main text we set $f_{ij}(r) = g_{ij}(r) + h_{ij}(r)(r - \overline{R}\eta_{ij})$.

S2. ADDITIONAL RESULTS

In Figs. S14a, S15a, 5a, and 6a we show phase diagrams with lines indicating the limits of metastability on heating and cooling at fixed ΔH. The calculations which these lines are based on are shown in (Fig. S1, S3, S5 and S7).

In Figs. S14b-f, S15b-d, 5b-h, 6b-h, 7b-j, 8a-j, and 10b-f of the main text we report the fraction of high spins as temperature varies The corresponding heat capacities, which provide a more sensitive signature of phase transitions and crossovers in SCO materials, are shown in Fig. S2b-f, S4b-d, S6b-h, S8b-h, S9b-j, S10a-j, and S12b-f respectively.

Lastly, in the main text we show the phase diagram for the next nearest neighbour $1n14$ family lattice model with $k_1 < 1$, $k_2 = 1.2|k_1|$ (Fig. 8, see also Fig. S8). In Fig. S13 we show phase diagram for the nearest neighbour model with $k_1 < 1$, $k_2 = 0.6|k_1|$ demonstrating the importance of the relative contributions of the magnitudes of k_1 and k_2 on the thermodynamics.

S2.1. NEAREST-NEIGHBOUR INTERACTIONS

In this section, we consider only the nearest-neighbour elastic interaction, k_1. That is, we set $k_2 = k_3 = k_4 = k_5 = 0$. The stability of the lattice requires $k_1 > 0$.[3] The phase diagram of this model is shown in Fig. S14a. As individual materials have constant ΔH, rather than constant ΔG, we mark lines of constant ΔH on the phase diagram and report the thermodynamic properties at selected values of ΔH (Figs. S14b-f).

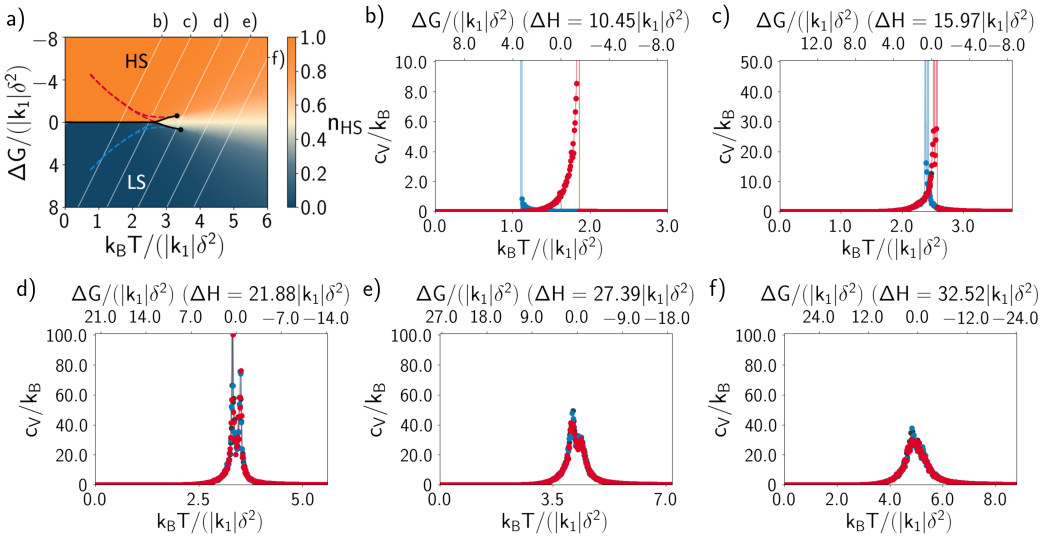

FIG. S2. (a) The phase diagram for nearest-neighbour interactions, $k_1 > 0$, reprinted from Fig. 4a for convenience. The colours indicate the equilibrium values for the fraction of high-spin metal centres, n_{HS}, calculated via parallel tempering. We find a (black) line of first order transitions that bifurcates at a triple point and ends in two critical points (black dots). There is no spontaneously broken symmetry or long-range order in the region between the two first order lines where $n_{HS} \simeq 1/2$. The blue (red) dashed line marks the limit of metastability for on the HS (resp. LS) phases on cooling (resp. heating), see Fig. S1. Individual materials have fixed ΔH (not fixed ΔG); the white lines are lines of constant ΔH and their labels correspond to panels (b-f) where the heat capacity, c_V, is plotted along these lines (see Fig. 4 for the corresponding high spin fractions). In these plots the blue, red and black lines represent the cooling, heating and equilibrium values respectively.

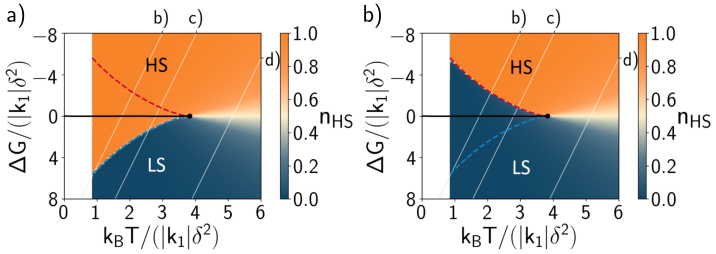

FIG. S3. The HS fraction, n_{HS}, calculated on (a) cooling and (b) heating for the next nearest neighbour square lattice model with $k_2 = 0.1k_1 > 0$. Lines and dots have the same meanings as in Fig. S2a. See Fig. S4a for the full phase diagram.

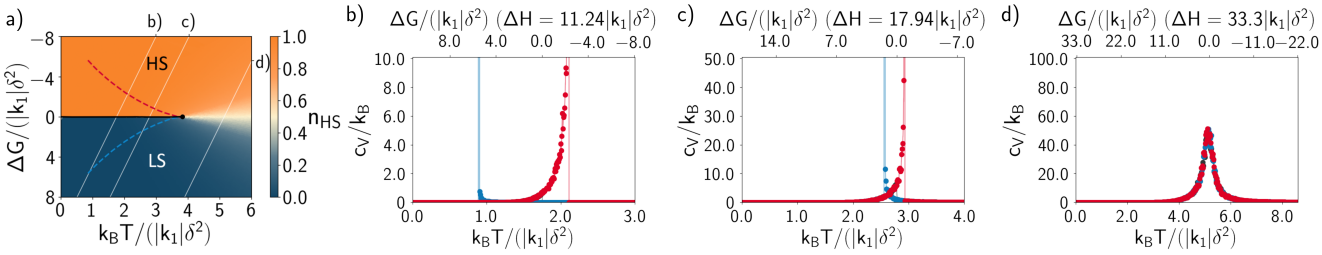

FIG. S4. (a) Phase diagram for the next nearest neighbour square lattice model with $k_2 = 0.1k_1 > 0$ reprinted from Fig. S15a for convenience. Lines and dots have the same meanings as in Fig. S2a. (b-d) The heat capacity, c_V, (see Fig. S15 for the corresponding HS fractions). Blue, red and black lines show data for the cooling, heating and thermal equilibrium predictions, respectively.

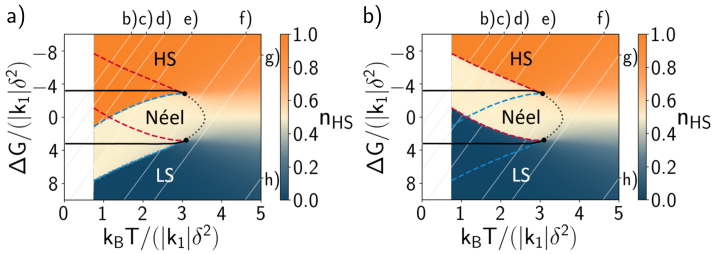

FIG. S5. The HS fraction, n_{HS}, calculated on (a) cooling and (b) heating for the next nearest neighbour square lattice model with $k_1 > 0$ and $k_2 = -0.2k_1$, appropriate for the $1n24$ and $1n02$ families. Lines and dots have the same meanings as in Fig. S2a. See Fig. S6a for the full phase diagram.

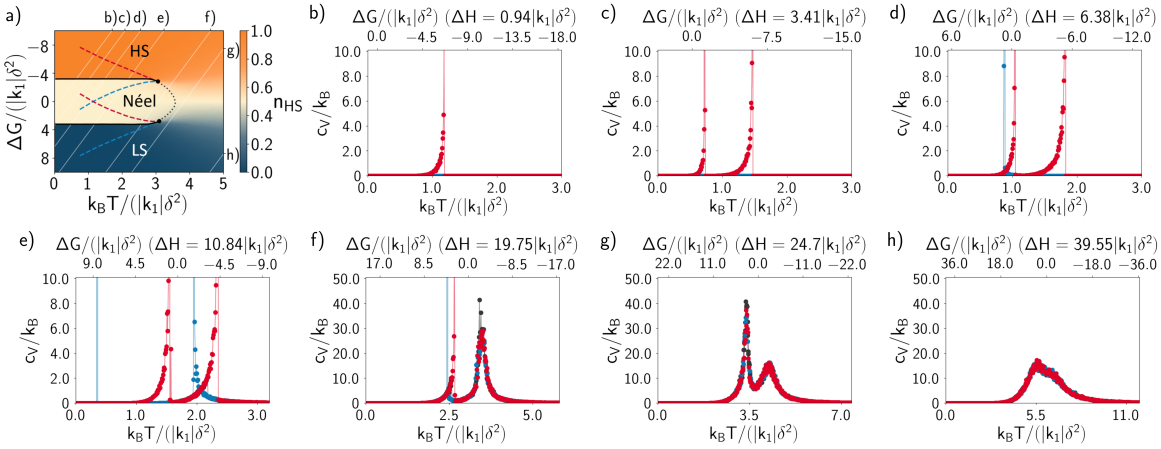

FIG. S6. (a) Phase diagram for the next nearest neighbour square lattice model with $k_1 > 0$ and $k_2 = -0.2k_1$, appropriate for the $1n24$ and $1n02$ families, reprinted from Fig. 5a for convenience. Lines and dots have the same meanings as in Fig. S2a. (b-h) The heat capacity, c_V, (see Fig. 5 for the corresponding HS fractions). Blue, red and black lines show data for the cooling, heating and thermal equilibrium predictions, respectively.

When the single molecule contribution to the free energy is much greater than the contribution of the cooperative elastic interactions, $\Delta H \gg k_1\delta^2$, we observe a gradual crossover (Figs. S14f and S2f). This thermodynamic behaviour is commonly reported in experiments on weakly cooperative materials.[4]

In the opposite regime, $\Delta H \ll k_1\delta^2$, we see a sharp one-step transition with hysteresis (Figs. S14b and S2b). This indicates a first order phase transition, as is commonly observed in bistable SCO materials.[4] Note that in our calculations the first order spin-state transition is not accompanied by a crystallographic phase transition, which is excluded by the symmetric breathing mode approximation.

In the intermediate regime, $\Delta H/(|k_1|\delta^2) \sim 15 - 30$, we see two-steps. Depending on the magnitude of $\Delta H/(|k_1|\delta^2)$

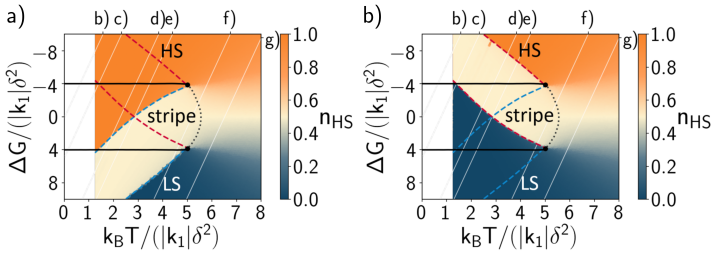

FIG. S7. The HS fraction, n_{HS}, calculated on (a) cooling and (b) heating for the next nearest neighbour square lattice model with $k_1 < 0$ and $k_2 = 1.2|k_1|$, appropriate for the $1n14$ family. Lines and dots have the same meanings as in Fig. S2a. See Fig. S8a for the full phase diagram.

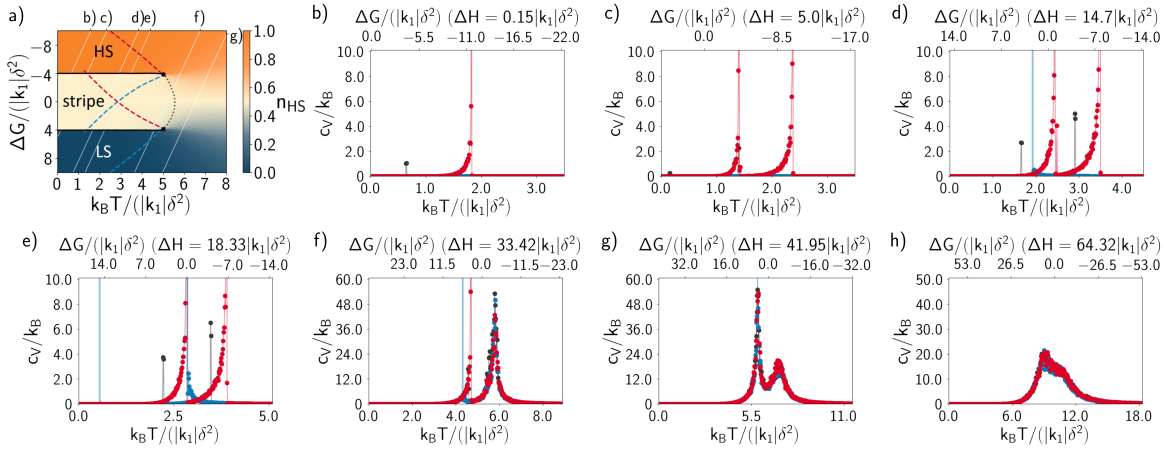

FIG. S8. (a) Phase diagram for the next nearest neighbour square lattice model with $k_1 < 0$ and $k_2 = 1.2|k_1|$, appropriate for the $1n14$ family, reprinted from Fig. 6a for convenience. Lines and dots have the same meanings as in Fig. S2a. (b-h) The heat capacity, c_V, (see Fig. 6 for the corresponding HS fractions). Blue, red and black lines show data for the cooling, heating and thermal equilibrium predictions, respectively.

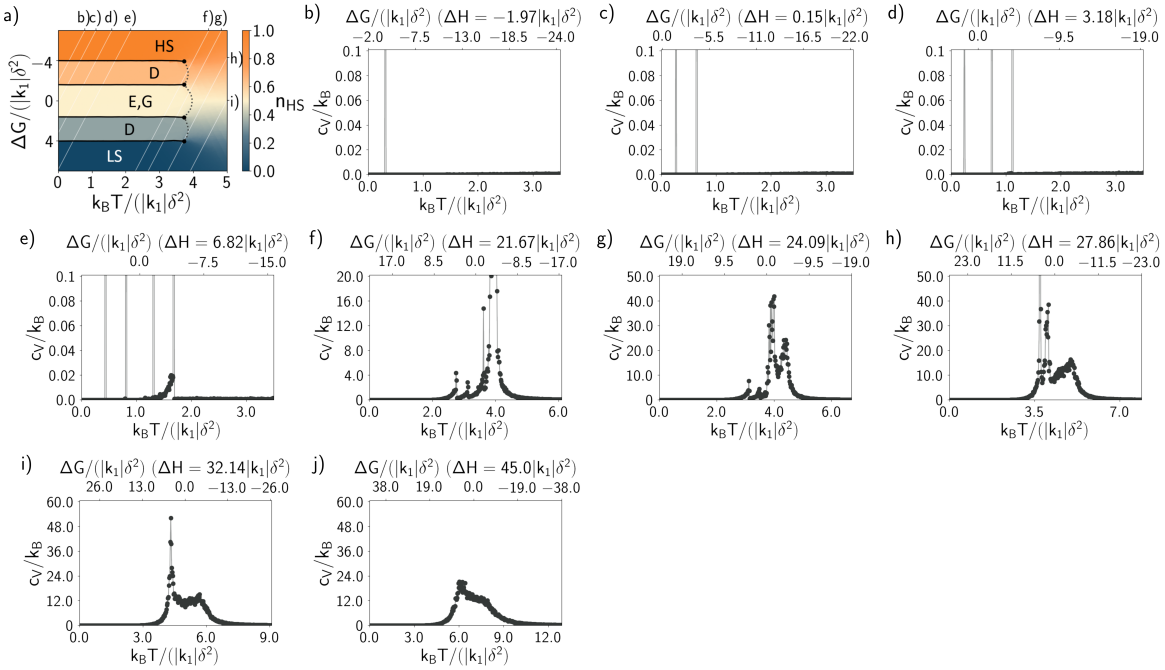

FIG. S9. (a) Phase diagram for the third nearest neighbour square lattice model with $k_1 > 0$, $k_2 = -0.9k_1$ and $k_3 = 0.5k_1$, appropriate for the $1n24$ and $1n02$ families, reprinted from Fig. 7a for convenience. Lines and dots have the same meanings as in Fig. S2a. (b-j) The heat capacity, c_V, (see Fig. 7 for the corresponding HS fractions). For simplicity only the parallel tempering results are shown.

these steps can occur as two first-order transitions with hysteresis (Figs. S14c and S2c), one first order transition and one crossover (Figs. S14d and S2d), or two crossovers (Figs. S14e and S2e). In between these regimes are critical points where the transitions become continuous.

The two-step behaviour is a result of the competition between the long-range strain and the elastic interactions. The elastic interactions favour an antiferroelastic phase with Néel ordering (Fig. 1a), whereas the long-range strain prefers all metal centres to be in the same spin-state. At $T = 0$ when $\Delta H = \Delta G > 0$ the LS phase is realized and for $\Delta H = \Delta G < 0$ the HS phase is energetically favourable. However, for $T = 0$ and $\Delta H = 0$ the Néel ordered state is degenerate with the HS and LS states (Figs. S14a and S1a). At sufficiently high temperatures thermal fluctuations stabilize short-range Néel correlations for $\Delta G \approx 0$, Figs. S14a and S2a. This cannot stabilise a true, long-range

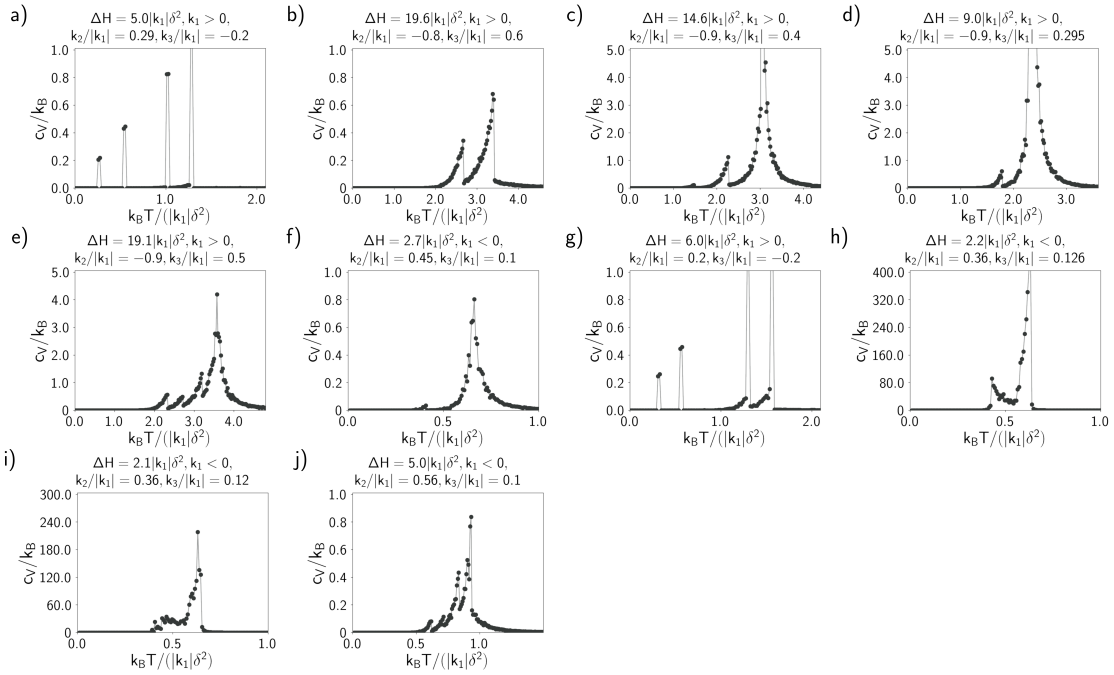

FIG. S10. Temperature dependence of the heat capacity in the third nearest neighbour model with the same parameters for which n_{HS} is plotted in Fig. 8. The parameters are reasonable for (a) $1n14$ family, (b-e) $1n24$ and $1n02$ families and (a-j) supramolecular lattices. For simplicity we only show the parallel tempering results.

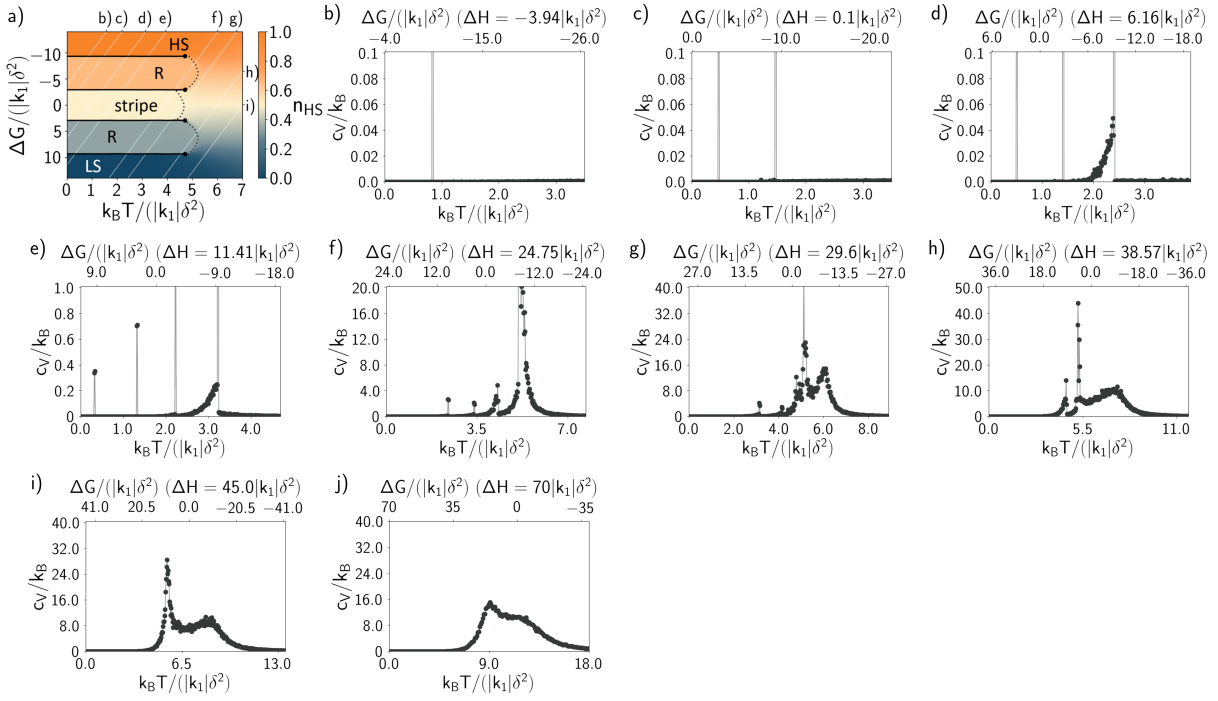

FIG. S11. (a) Phase diagram for the fifth nearest neighbour square lattice model with $k_1 < 0$, $k_2 = 1.2|k_1|$, $k_3 = -0.5|k_1|$, $k_4 = 0$, and $k_5 = 0.2|k_1|$, appropriate for the $1n14$ family, reprinted from Fig. S18a for convenience. Lines and dots have the same meanings as in Fig. S2a. (b-j) The heat capacity, c_V, (see Fig. S18 for the corresponding HS fractions). For simplicity only the parallel tempering results are shown.

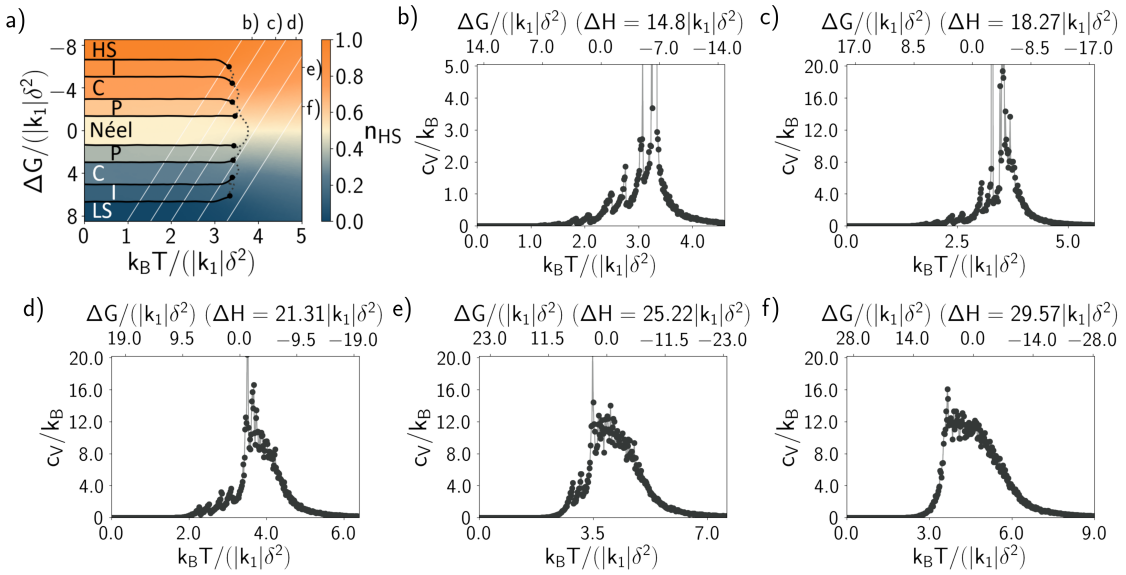

FIG. S12. (a) Typical slice of the finite temperature phase diagram all interactions up to fifth nearest neighbours. Lines and dots have the same meanings as in Fig. S2a. (b-f) The heat capacity, c_V (See Fig. 10 for the corresponding fraction of high spins). For simplicity only the parallel tempering predictions are shown.

ordered, Néel phase, but does result in a observed two-step transition, Figs. S14d and S2d. The same qualitative features of this phase diagram have been also been captured by Chenyshov *et al.* [5] using a Landau theory.

However, with only nearest neighbour interactions present, the Néel phase is the only antiferroelastic phase present. Furthermore, the Néel phase is observed only in an extremely narrow temperature range. Experimentally, many different antiferroelastic phases have been found and these phases can stable over relatively broad temperature ranges. This is consistent with the idea that longer range elastic interactions are vitally important for multistep transitions.

S2.2. STRICTLY POSITIVE NEXT NEAREST NEIGHBOUR INTERACTIONS (ANY FAMILY)

$k_1 > 0$ and $k_2 > 0$ is possible for any of the lattices shown in Fig. 2 provided that the minima of both interactions are roughly commensurate with a square lattice. At $T = 0$ the LS and HS states are separated by a first order phase transition at $\Delta G = 0$, Figs. 4a and S15a. For $T > 0$ this phase transition remains at $\Delta G = 0$ until it reaches a critical point, where the transition is continuous. Thus, the frustration has entirely suppressed the Néel order found at finite temperatures for $k_2 = 0$ (compare Figs. S14 and S15).

Considering lines of constant ΔH, which represent individual materials, we see three distinct thermodynamic behaviours: When the elastic interactions are strong compared to the single molecule physics, $\Delta H \ll |k_1|\delta^2$, the transitions are sharp and first-order, the width of the hysteresis is greater the smaller $\Delta H/|k_1|\delta^2$ is (Figs. S15b,c and S4b,c). If the elastic interactions are weak, $\Delta H \gg |k_1|\delta^2$, we find a crossover (Figs. S15d and S4d). These two regimes are separated by a continuous (or second order) phase transition at the critical point.

Consistent with this prediction, single step transitions are common and observed in all of the families of materials discussed here.

[1] J. Cruddas and B. J. Powell, Spin-State Ice in Elastically Frustrated Spin-Crossover Materials, *J. Am. Chem. Soc.*, 2019, **141**, 1970-19799.
[2] H.-Z. Ye, C. Sun and H. Jiang, Monte-Carlo simulations of spin-crossover phenomena based on a vibronic Ising-like model with realistic parameters, *Phys. Chem. Chem. Phys.*, 2015, **17**, 6801-6808.
[3] The lattice is stable to shear distortions because the symmetric breathing mode approximation is equivalent to assuming an infinite spring constant for shear modes.
[4] P. Gütlich, Y. Garcia and H. A. Goodwin, Spin crossover phenomena in Fe(II) complexes, *Chem. Soc. Rev.*, 2000, **29**, 419-427.

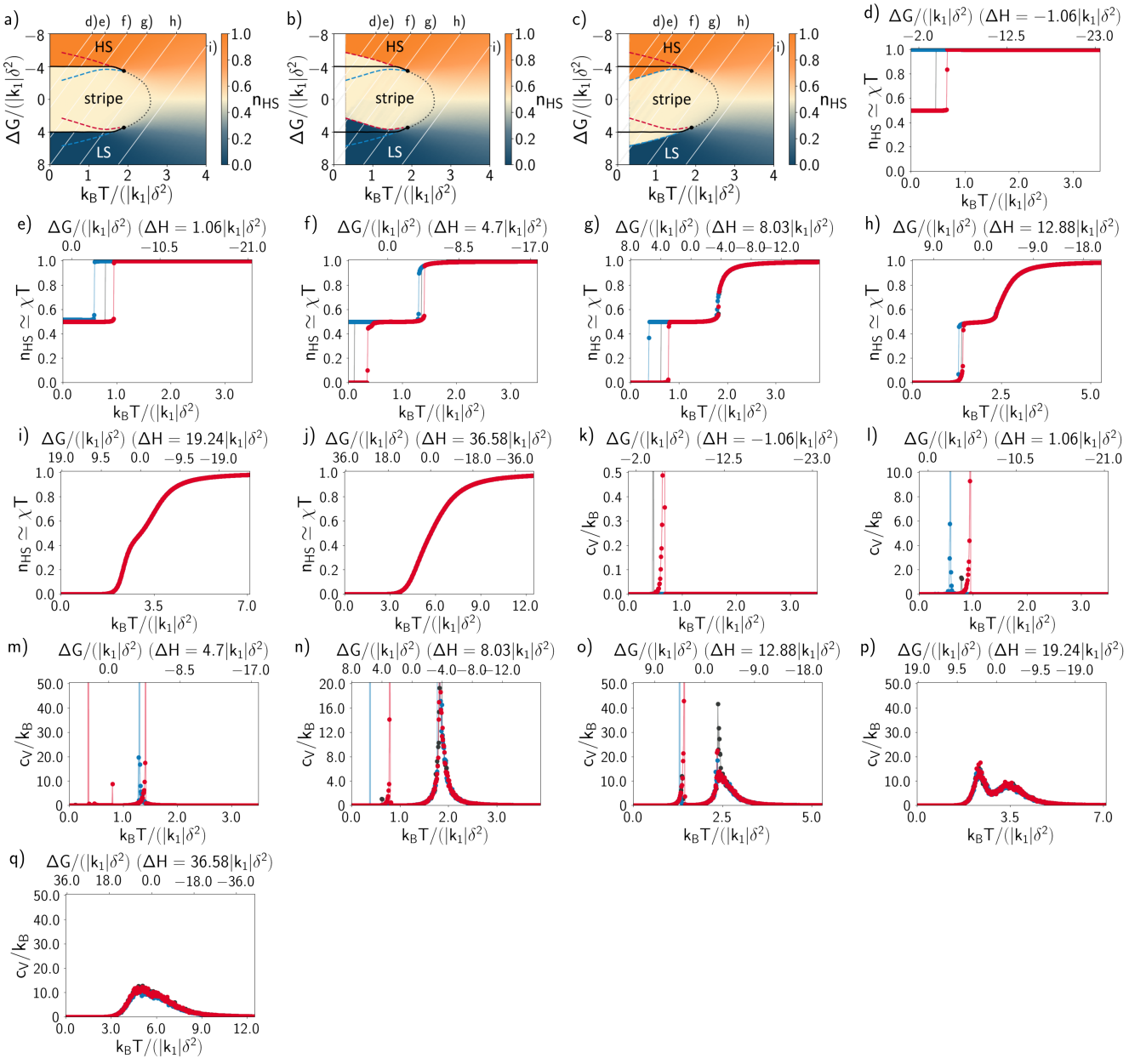

FIG. S13. (a) Phase diagrams for the next nearest neighbour model with $k_1 < 0$, $k_2 > 0$ (here we take $k_2 = 0.6|k_1|$, other parameters give similar results). Lines and dots have the same meanings as in Fig. S2a. The HS fractions calculated on (b) heating and (c) cooling with fixed ΔH are used calculate the limits of stability. Note that in contrast to the results for $k_1 > 0$ and $k_2 > 0$ the relative magnitudes of k_1 and k_2 has importance consequences for the observed behaviours (see, e.g., Figs. 6 and S8). (d-j) The fraction of high spins, n_{HS} and (k-q) the corresponding heat capacities. Blue, red and black lines show data for the cooling, heating and thermal equilibrium predictions, respectively.

[5] D. Chernyshov, H.-B. Bürgi, M. Hostettler, and K. W. Törnroos, Landau theory for spin transition and ordering phenomena in Fe(II) compounds, *Phys. Rev. B*, 2004, **70**, 094116-094124.

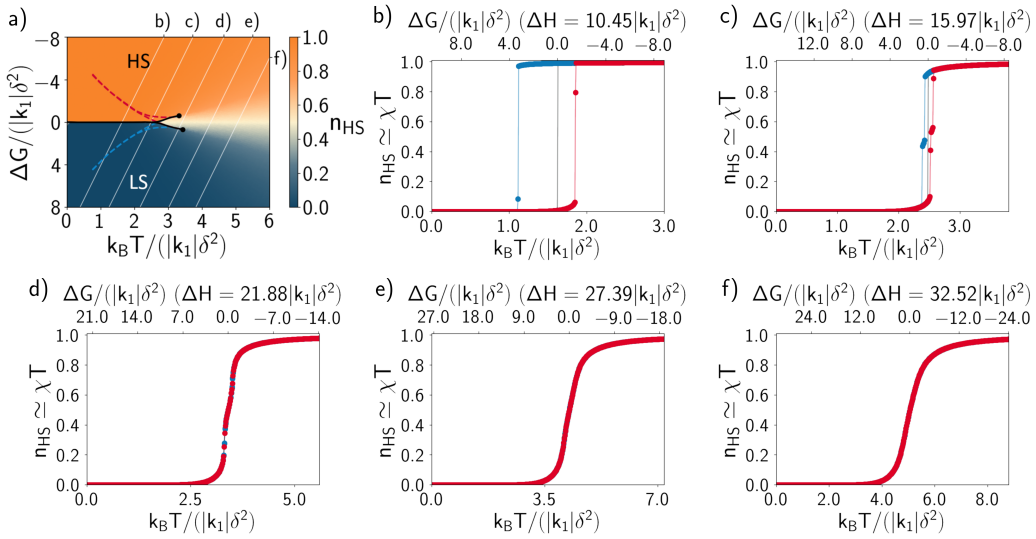

FIG. S14. (a) The phase diagram for nearest-neighbour interactions, $k_1 > 0$. Colours in the phase diagram indicate the fraction of high-spin M sites, $n_{HS} \sim \chi T$ where χ is the susceptibility, calculated via parallel tempering. The (black) line of first order transitions bifurcates at a triple point and ends in two critical points (black dots). There is no spontaneously broken symmetry or long-range order in the region between the two first order lines where $n_{HS} \simeq 1/2$. The blue (red) dashed line marks the limit of metastability for the HS (resp. LS) phases on cooling (resp. heating), cf. Fig. S1, and show the width of the hysteresis. Individual materials have fixed ΔH, white lines correspond to panels (b-f), where the fraction of high spins is plotted (see Fig. S2 for the corresponding heat capacities). In these plots the blue, red and black lines represent the cooling, heating and parallel tempering values respectively.

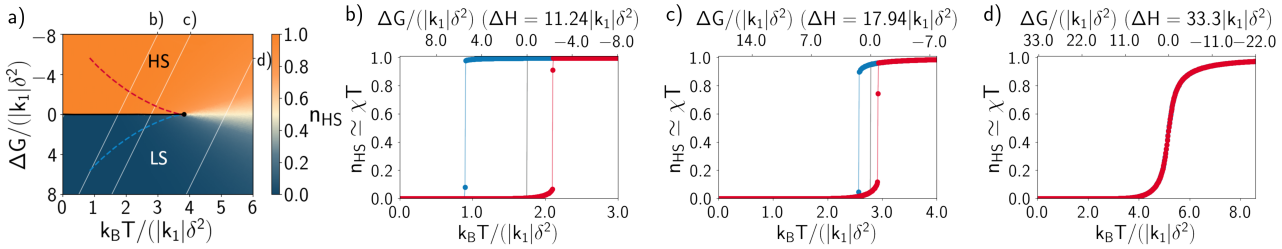

FIG. S15. (a) Typical phase diagram for the next nearest neighbour square lattice model with k_1 and $k_2 > 0$ (here $k_2 = 0.1k_1$; see also Fig. S3). (b-d) The fraction of high spins, n_{HS} (see Fig. S4 for the corresponding heat capacities). Symbols have the same meanings as in Fig. S14.

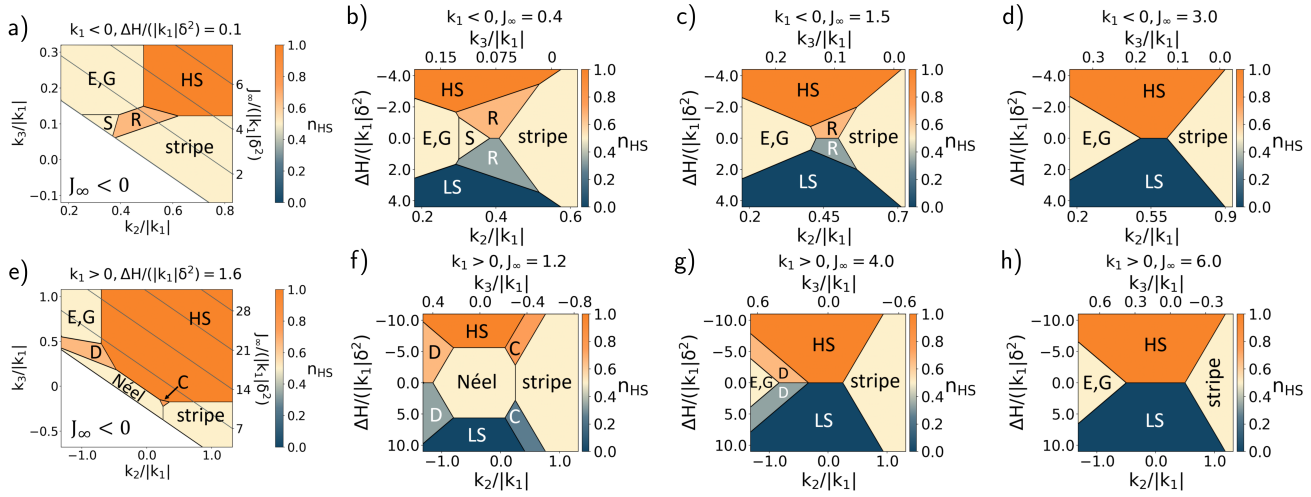

FIG. S16. Slices of the zero-temperature phase diagram with up to third nearest-neighbour elastic interactions k_1, k_2 and k_3 for (a,e) constant ΔH and (b-d,f-h) constant J_∞. Grey lines in (a,e) indicate lines of constant J_∞. In addition to the phases that are energetically preferred by individual elastic interactions (HS, LS, Néel, stripe, C, E and G), frustration introduces additional phases into the zero-temperature phase diagram (D, R and S). E, G indicates that the E and G phases are degenerate.

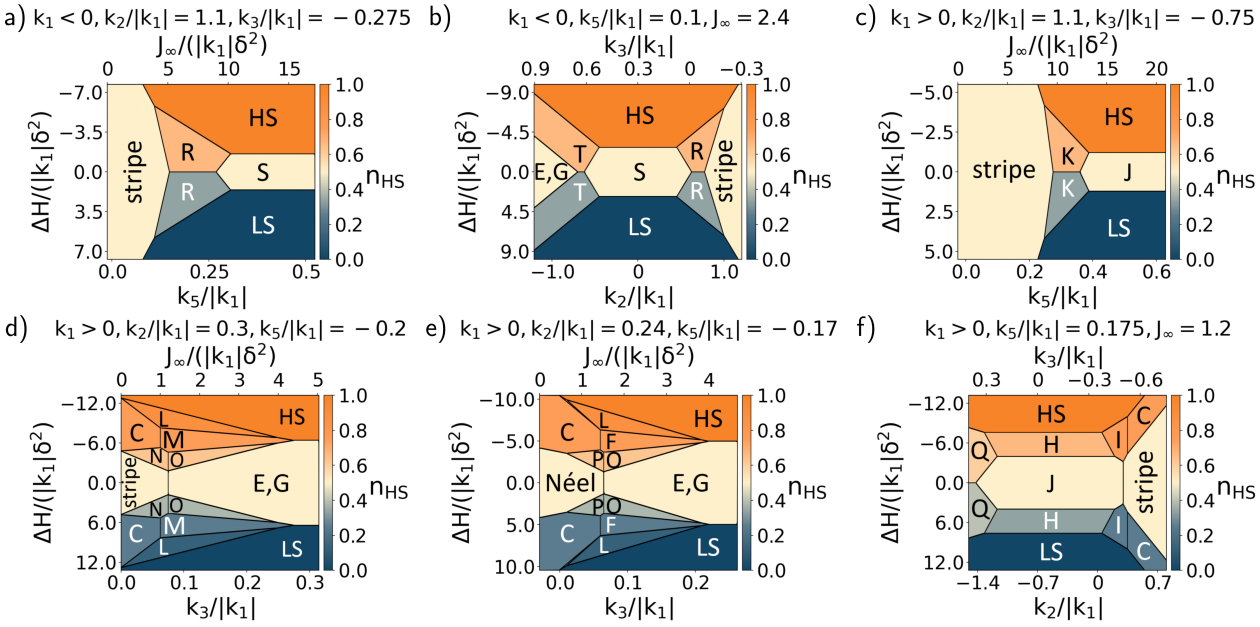

FIG. S17. Selected slices of the zero temperature phase diagram with up to fifth nearest-neighbour interactions showing thirty-six distinct phases. In general increasing the number of nearest-neighbour interactions increases the complexity of the phase diagram.

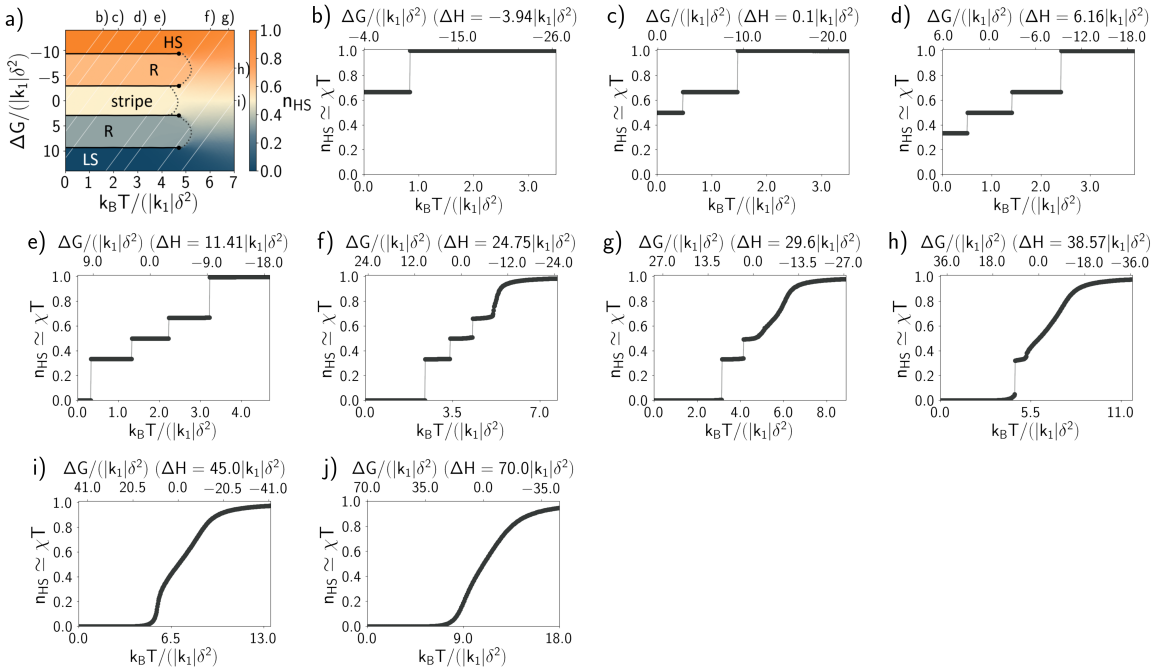

FIG. S18. (a) Typical phase diagram for the $1n14$ family with $k_1 < 0$, $k_2 > 0$, $k_3 < 0$, $k_4 = 0$ and $k_5 > 0$ (here $k_2 = 1.2|k_1|$, $k_3 = -0.5|k_1|$ and $k_5 = 0.2|k_1|$). The R phase consists of alternating stripes of width 2 and width 1 (Fig. 1). Lines and dots have the same meanings as in Fig. S2a. (b-i) The fraction of high spins, n_{HS} (see Fig. S11 for the corresponding heat capacities). Only the parallel tempering Monte Carlo predictions are reported.